APPLIED ORGANOMETALLIC CHEMISTRY
*Appl. Organometal. Chem.* 2005; **19**: 530–537
Published online in Wiley InterScience (www.interscience.wiley.com). DOI:10.1002/aoc.857



# Field-effect transistor based on organosoluble germanium nanoclusters†

**Akira Watanabe,[1]* Fusao Hojo[2] and Takao Miwa[2]**

[1]Institute of Multidisciplinary Research for Advanced Materials, Tohoku University, Katahira, Aoba-ku, Sendai 980-8577, Japan
[2]Hitachi Research Laboratory, Hitachi, Ltd, Ibaraki, Hitachi 319-1292, Japan

Received 4 July 2004; Revised 10 August 2004; Accepted 24 September 2004

**The structural and electrical properties of organosoluble germanium nanoclusters are studied. The organogermanium nanocluster (OGE) is a polygermane with a three-dimensional $\sigma$-conjugated chain. The OGE is prepared from $GeCl_4$ by a simple one-pot reaction, where the germanium nanocluster is obtained by the reaction of $GeCl_4$ using magnesium metal and the capping reaction of the chlorine group by an alkyl Grignard reagent in tetrahydrofuran. The optical energy gap of the *tert*-butyl-substituted OGE is lower than that of the *n*-propyl-substituted OGE, corresponding to the higher molecular weight and the larger extent of the $\sigma$-conjugation along the Ge–Ge chain. The conductivity of the OGE is enhanced by heat treatment, which induces the elimination of organic substituents, the reconstruction of the Ge–Ge chain, and the extension of a three-dimensional germanium network among germanium clusters. The field-effect transistor fabricated by a coating technique using the *tert*-butyl-substituted OGE shows signal amplification properties. Copyright © 2005 John Wiley & Sons, Ltd.**

**KEYWORDS:** polygermane; germanium nanocluster; field-effect transistor

## INTRODUCTION

Polysilane (polysilylene) and polygermane (polygermylene) are $\sigma$-conjugated polymers that have a one-dimensional Si–Si and Ge–Ge chain, respectively. Various kinds of $\sigma$-conjugated polymer have been synthesized,[1–10] and the optical and electrical properties are classified based on the dimensionality of the $\sigma$-conjugated chain.[6] In previous papers, we have reported the formation of inorganic films using organosilicon nanocluster (OSI) and organogermanium nanocluster (OGE) as precursors.[11–17] These polymers are hyperbranched polysilanes and polygermanes and have three-dimensional $\sigma$-conjugated chains. The OSI and OGE were prepared from $SiCl_4$ and $GeCl_4$ respectively by a simple one-pot reaction, where the nanoclusters of silicon (germanium) were obtained by the reaction of $SiCl_4$ ($GeCl_4$) using magnesium metal in tetrahydrofuran (THF) and the capping reaction of the remaining chlorine group by an alkyl Grignard reagent in THF. The molecular weight and the structure of the OGE are influenced remarkably by the type of organic substituent, because the organic substituent solubilizes the germanium cluster core in solution. The OGE shows excellent solubility and processability due to the amorphous germanium skeleton in comparison with the germanium nanocrystals.[18–20] In this study, we investigate the influence of the organic side chain on the structural and electrical properties of the OGE. The OGE was applied to the active material for a field-effect transistor (FET) and the signal amplification properties of the FET were demonstrated. The solution-processable organic semiconductors represent a cost-effective alternative to conventional silicon technology, where the preparation of the silicon thin film is mainly based on the deposition of reactive species on a substrate from the gas phase.[21–25] However, one of the problems in the commercial application of an organic semiconductor to an electronic device is the instability in comparison with the inorganic semiconductor. The OGE has solution processability and a stable inorganic germanium can be prepared by heat treatment of the OGE to eliminate the

*Correspondence to: Akira Watanabe, Institute of Multidisciplinary Research for Advanced Materials, Tohoku University, Sendai 980-8577, Japan.
E-mail: watanabe@tagen.tohoku.ac.jp
†Dedicated to the memory of Professor Colin Eaborn who made numerous important contributions to the main group chemistry.
Contract/grant sponsor: Ministry of Education, Culture, Sports, Science and Technology of Japan; Contract/grant number: 15550179.

organic substituents. This method using OGE as a precursor provides a new process for the formation of a stable semiconducting material.

## EXPERIMENTAL

### Materials

The OGEs were obtained by the reaction of $GeCl_4$ using magnesium metal in THF and the capping reaction of the remaining Ge–Cl group by alkyl Grignard reagents in THF at the end of the reaction (Scheme 1).[12,13,15]

The polymerization of 16 mmol $GeCl_4$ in 40 ml THF with magnesium metal (128 mmol) at 10 °C under an argon atmosphere and ultrasonic field (40 W) gave a dark dispersion in THF. Solubilization of the germanium core was achieved by the substitution of the chlorine group of the germanium core with an organic group as follows. After the reaction for 90 min, a 16 mmol alkylbromide (*n*-propyl- or *tert*-butyl-bromide) was added dropwise into the dispersion at 10 °C under an ultrasonic field. The reaction of alkylbromide with the remaining magnesium metal gave the Grignard reagent and it replaces the chlorine atom around the germanium core with an alkyl group. After reaction at 10 °C for 60 min, an additional 16 mmol alkylbromide was added dropwise to the reactants, and the substitution reaction proceeded at 50 °C for 2 h. After the above procedures, the reaction mixtures were stirred overnight at room temperature, and then the solution and the precipitates were separated by decantation. The decanted solution was poured into methanol (MeOH) and the alkyl-substituted germanium nanocluster was obtained as a precipitate. In the case of the *n*-propyl-substituted OGE, the precipitate was purified by column chromatography using silica gel and non-polar *n*-hexane as the eluent to remove the oxidized products. After the evaporation of the *n*-hexane eluent, the *n*-propyl-substituted OGE was obtained as a pale yellow powder. In the case of *tert*-butyl-substituted OGE, the major products were insoluble in *n*-hexane; therefore, the crude products were purified as follows. First, the low-molecular-weight components were extracted using *n*-hexane as a solvent. The residue was dissolved into toluene and purified by reprecipitation using MeOH as a precipitant. The *tert*-butyl OGE was obtained as a red powder. Thin films of OGEs (*ca* 0.3 μm) were prepared by spin coating of a 5 wt% toluene solution on a substrate. The films were heat-treated at various temperatures for 30 min *in vacuo* (*ca* $10^{-6}$ Torr).

### Measurements

The weight-average molecular weight $M_w$, number-average molecular weight $M_n$, and the molecular weight distributions $M_w/M_n$ of OGEs were determined by gel permeation chromatography (GPC) using monodispersed polystyrenes as standards. The $^1H$ NMR spectra were recorded on a JEOL Lambda400. The FT-IR spectra were observed using a JEOL JIR-100). Raman spectra were measured by a micro-Raman apparatus with a spectrometer and a liquid-nitrogen-cooled charge-coupled device detector. All samples were excited with the 488 nm line available from an argon-ion laser. The thicknesses of the films were determined by an electromechanical stylus instrument. The conductivities of the OGE films heat-treated at various temperatures were observed for samples with two gold electrodes vacuum-deposited onto the heat-treated OGE film on a quartz substrate through a comb-shaped patterned metal mask with a gap of 0.1 mm. An FET device was fabricated from the heat-treated OGE film. The OGE was spin-coated on a silicon substrate (n-type, ⟨100⟩, 0.02 Ω cm) which has a 600 nm thickness insulating layer of $SiO_2$ on the top, where a thick $SiO_2$ layer was used to prevent the breakdown of the device. After the heat treatment of the OGE–$SiO_2$–Si substrate *in vacuo*, two comb-shaped patterned gold electrodes were vacuum-deposited on the OGE film.

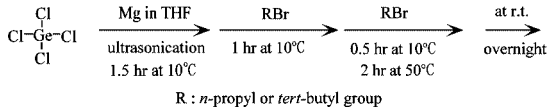


**Scheme 1.** Synthetic route to OGEs.

## RESULTS AND DISCUSSION

### Characterization of OGEs

The molecular weight distribution of the *tert*-butyl-substituted OGE determined by GPC analysis was broad, with maxima around 2000 and 7000 tailing to higher molecular weights than 100 000 as shown in Fig. 1b. On the other hand, *n*-propyl-substituted OGE showed a monomodal molecular weight distribution (Fig. 1a), where $M_w$ and $M_w/M_n$ are 1920 and 1.16, respectively. This difference can be explained by considering that the bulky *tert*-butyl group effectively surrounds and solubilizes the larger germanium clusters in an organic solvent compared with the *n*-propyl group. The *tert*-butyl-substituted OGE shows a shoulder peak as shown in Fig. 1b. This feature is similar to polysilanes prepared by the Kipping reaction of organochlorosilane using sodium.[26] Both reactions proceed at the surface of the magnesium (sodium) metal and in the solution. Such an inhomogeneous reaction induces the broad molecular weight distribution.

In previous papers,[9,17] the diameters of the OSI were estimated by considering the size of the monodispersed polystyrenes that were employed as standards in the determination of the molecular weight of the OSI using size-exclusion chromatography. Littau and co-workers.[27] have reported on the comparison of the sizes of surface-oxidized silicon nanocrystals determined by transmission electron microscopic (TEM) analysis and size exclusion chromatography, and showed good agreement between the two methods. The size of a polystyrene can be estimated from the equation for the radius of gyration, $s_o = r_o/6^{0.5} = 0.0685\, M_n^{0.5}/6^{0.5}$, where $r_o$ is the end-to-end

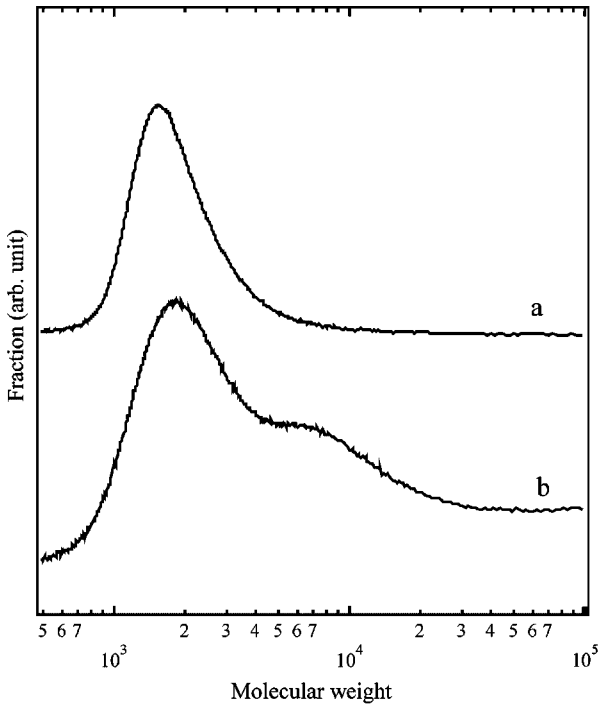


**Figure 1.** Molecular weight distributions of (a) *n*-propyl-substituted OGE and (b) *tert*-butyl-substituted OGE.

distance of the polymer chain.[28] The size for the *n*-propyl-substituted OGE with narrow molecular weight distribution was estimated to be 2.3 nm in diameter, where the germanium cluster size is smaller than the estimated value without the correction for the organic side chains. In the case of the *tert*-butyl-substituted OGE, the estimation of the size is difficult because of the broadness of the molecular weight distribution. Assuming monodispersion of the molecular weight ($M_w/M_n = 1$) for the two peaks at 2000 and 7000 in Fig. 1b, the sizes are calculated to be 2.5 nm and 4.7 nm, respectively. These values are smaller than those reported for surface-functionalized germanium nanoparticles.[18–20,29] Kauzlarich and co-workers have reported the solution-based synthesis of crystalline germanium nanoparticles via the Zintl salt reduction procedure.[18–20] The metathesis of the Zintl salts NaGe, KGe, and $Mg_2Ge$ with $GeCl_4$ in boiling glymes have been used to prepare germanium nanoparticles. By the addition of a variety of organic functionalities to the surface of the germanium nanoparticle, a clear suspension of the germanium nanoparticles from 2 to 10 nm in diameter can be formed.[18–20] The preparation of the alkyl-surface-functionalized germanium particle by the reduction of $GeI_4$ using $LiAlH_4$ has also been reported by Veinot and co-workers.[29] The electron diffraction pattern of the germanium nanoparticle was consistent with crystalline germanium. The size distribution of the particles was within the range of 2–7 nm from TEM analysis. The remarkable difference between the OGE and the germanium nanoparticles reported by the Kauzlarich and Veinot groups is the feature of the germanium skeleton, where the former is amorphous[14,15] and the latter is crystalline. Such a difference must be caused by the reaction conditions. The condition of the OGE synthesis is milder than that of the crystalline germanium nanoparticles. The former is the reduction of $GeCl_4$ using magnesium at 10 °C, and the latter is the reduction of Zintl salts in boiling glymes or the reduction of $GeI_4$ using $LiAlH_4$. The smaller size of the OGE must be due to the mildness of the reaction conditions.

From the elemental analyses, the compositions of the *n*-propyl- and *tert*-butyl-substituted OGEs are determined to be $Ge_1(C_3H_7)_{1.45}$ and $Ge_1(C_4H_9)_{0.41}$, respectively. The germanium cluster can be solubilized by the *tert*-butyl groups with a smaller substitution rate than that of the *n*-propyl groups. On the other hand, the bulkiness reduces the substitution efficiency of the bromine group with the *tert*-butyl group. In Fig. 2b, the FT-IR spectrum of the *tert*-butyl-substituted OGE shows the band assigned to Ge–H to be around 2000 $cm^{-1}$. The Ge–H bonds are formed by the well-known reducing ability of *tert*-butyl Grignard reagents, which often act as $\beta$-hydride donors. On the other hand, because of the purification by column chromatography using silica gel and non-polar *n*-hexane as the eluent, the *n*-propyl-substituted OGE shows no signal assigned to Ge–H. In the case of the *tert*-butyl-substituted OGE, purification by chromatography was not effective at removing the components with Ge–H. The skeleton of the germanium

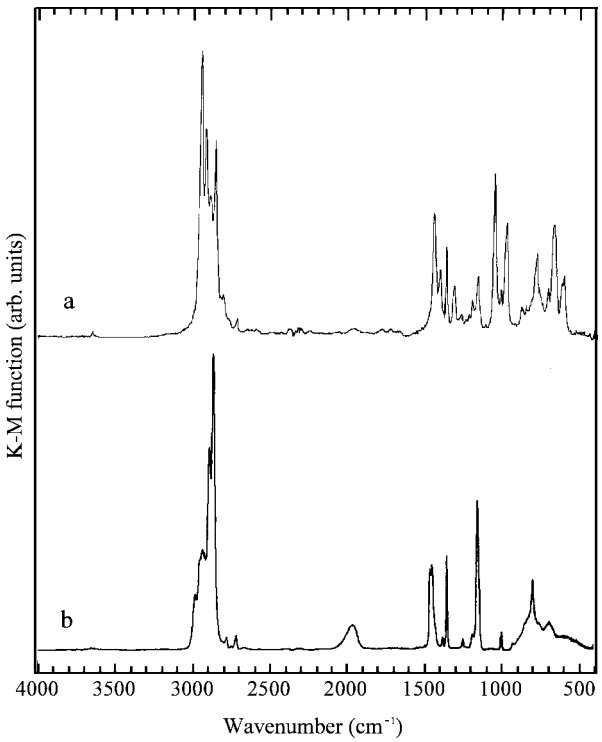


**Figure 2.** FT-IR spectra of (a) *n*-propyl-substituted OGE and (b) *tert*-butyl-substituted OGE.

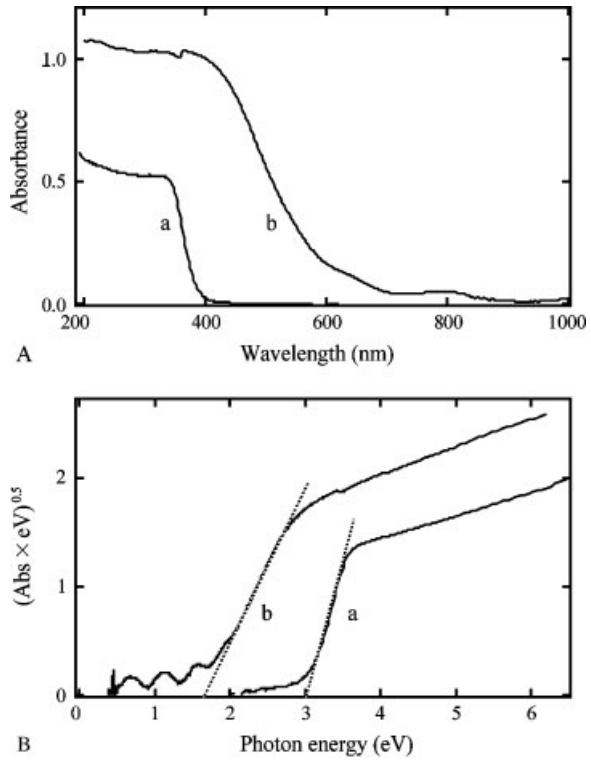


**Figure 3.** Absorption spectra (A) and the Tauc plots (B) of (a) *n*-propyl-substituted OGE and (b) *tert*-butyl-substituted OGE.

cluster can be assigned as amorphous because of the broad Raman band of the Ge–Ge lattice, as is described later.

Figure 3 shows the absorption spectra and the Tauc plots for *n*-propyl- and *tert*-butyl-substituted OGE films spin-coated on a quartz substrate. The absorption spectra of $\sigma$-conjugated polymers such as polysilanes and polygermanes are strongly influenced by the main chain structure. With increasing $\sigma$-conjugation length, the absorption band shifts to longer wavelengths (lower energy region). The dimensionality of the $\sigma$-conjugated chain also influences the optical properties.[17] With increasing $\sigma$-conjugated branching chain and the network structure, a sharp absorption spectrum of a linear $\sigma$-conjugated chain in the UV region changes into a broad one accompanying the shift of the absorption edge to longer wavelengths. In the case of the $\sigma$-conjugated Si–Si chain, the branched and network Si–Si chains were prepared by using trichloroorganosilane as a monomer. The OSI synthesized from tetrachrolosilane monomer has a three-dimensional structure and shows the lowest transition energy for absorption and emission spectra.[17] The polygermanes also show a similar tendency.[13,15] Another factor that influences the optical properties of the $\sigma$-conjugated chain is the size effect as reported for the OSI.[17] As shown in Fig. 3, OGEs also showed the size effect, where the wavelength of the absorption edge of the *tert*-butyl-substituted OGE is longer than that of the *n*-propyl-substituted OGE. From the intercept of the tangent line of the Tauc plots (Fig. 3B), the optical band gaps for the *n*-propyl- and *tert*-butyl-substituted OGEs were determined to be 3.0 eV and 1.7 eV, respectively. The extremely low optical band gap of the *tert*-butyl-substituted OGE suggests a large extent of $\sigma$-conjugation along the Ge–Ge chain.

## Electrical properties

The Raman scattering provides a convenient means for analyzing the structure of the Ge–Ge lattice. The amorphous germanium (*a*-Ge) and crystalline germanium (*c*-Ge) show broad and sharp transverse optical (TO) phonon bands around 280 $cm^{-1}$ and 298 $cm^{-1}$, respectively.[30–33] The Raman bands of *n*-propyl- and *tert*-butyl-substituted OGEs heat-treated at various temperatures are shown by dotted and solid lines, respectively in Fig. 4. The germanium skeleton of the *n*-propyl-substituted OGE without heat treatment is amorphous judging from the broad TO-phonon band. The *tert*-butyl-substituted OGE showed a rather sharp band around 300 $cm^{-1}$ with a broad band around 180 $cm^{-1}$. After heat treatment at 300 °C, these Raman bands broadened and shifted to 280 $cm^{-1}$, which are similar to inorganic *a*-Ge. Such spectral changes can be assigned to the reconstruction of the Ge–Ge lattice accompanying the thermal decomposition of

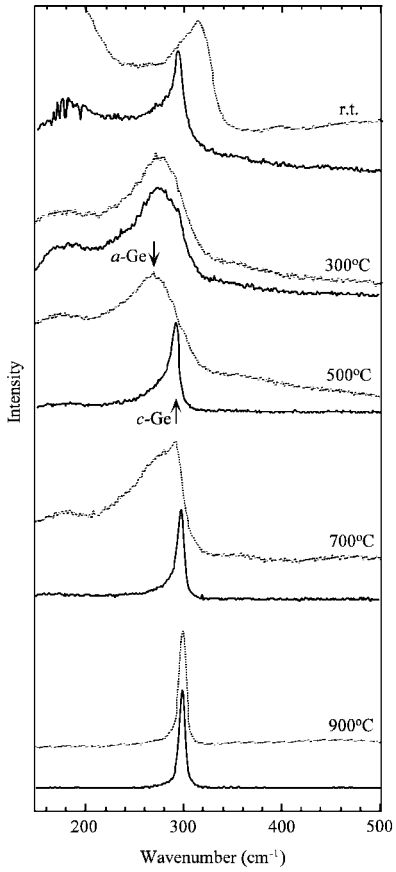


**Figure 4.** Raman spectra of OGEs heat-treated at various temperatures for *n*-propyl-substituted OGE (dotted line) and *tert*-butyl-substituted OGE (solid line).

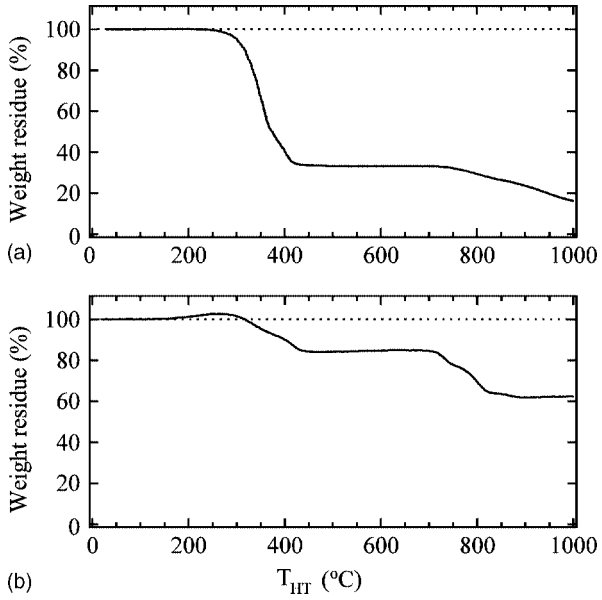


**Figure 5.** TG curves of (a) *n*-propyl-substituted OGE and (b) *tert*-butyl-substituted OGE.

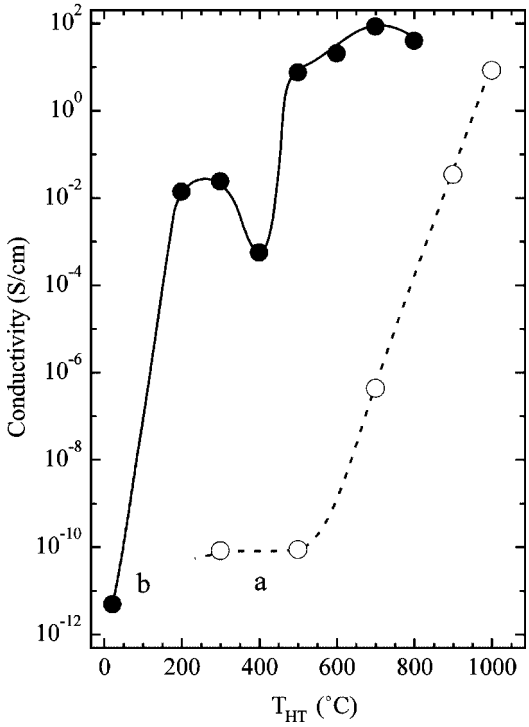


**Figure 6.** Effect of the heat-treatment temperature on the conductivity at 22 °C for (a) *n*-propyl-substituted OGE and (b) *tert*-butyl-substituted OGE.

the organic side chains judging from the thermogravimetric (TG) curves (Fig. 5). 300 °C is the temperature where the weight loss starts for both OGEs, as shown in Fig. 5.

The Raman spectra of the *tert*-butyl-substituted OGE heat-treated at 500 °C showed a narrow band tailing to lower wavenumbers, which can be assigned to a polycrystalline germanium. On the other hand, the Raman band of the *n*-propyl-substituted OGE heat-treated at 500 °C is still broad and attributed to *a*-Ge. In the case of *n*-propyl-substituted OGE, the crystallization of the germanium lattice was observed above 700 °C. The *tert*-butyl-substituted OGE was crystallized at a lower temperature than the *n*-propyl-substituted OGE, which is due to the large molecular weight and the extent of the Ge–Ge chain of the former. The lower ratio of the organic side chains to germanium atoms for the *tert*-butyl-substituted OGE than that for *n*-propyl-substituted OGE is also advantageous to the reconstruction and the crystallization of the germanium lattice eliminating the organic side chains. After heat treatment above 900 °C, crystallization was observed for both OGEs. Two transition regions around 350 and 750 °C appear in the $T_G$ curves of both OGEs. The first weight-loss region around 350 °C corresponds to the decomposition of the organic side chains, judging from the disappearance of their Raman band.[13] The second weight-loss region around 750 °C may be related to the reconstruction of the germanium lattice, where the weight loss is caused by the exclusion of oxidized segments from the germanium lattice during crystallization.

The electrical conductivities of OGE films are plotted against the heat treatment temperatures in Fig. 6. Without heat treatment the OGE film is almost an insulator, because the $\sigma$-conjugation along the Ge–Ge chain is isolated by organic substituents and the intramolecular charge carrier transport among the clusters is inhibited. In a previous paper[34] we depicted one of the possible structures of the OSI molecule as being a silicon cluster surrounded by organic groups and the isolation of the $\sigma$-conjugated Si–Si chain in solids. A similar isolation effect by organic substituents should be considered for the OGE. The heat treatment induces the elimination of organic substituents and the reconstruction of the Ge–Ge chain, which cause the extension of a three-dimensional germanium network among germanium clusters. In the case of the *tert*-butyl-substituted OGE, the conductivity increased by 10 orders of magnitude by heat treatment at 200 °C. The highest conductivity was observed at 700 °C, because the formation of large crystal grains above 800 °C induces discontinuities in the film. The structure of the precursor the conductivity of the heat-treated film remarkably influences. The conductivity of the *n*-propyl-substituted OGE is lower than that of *tert*-butyl-substituted OGE, corresponding to a lower crystallinity in the former than in the latter.

## FET based on OGE

An FET device was fabricated from the heat-treated OGE film. The OGE was spin-coated on a silicon substrate that has a 600 nm thickness insulating layer of $SiO_2$ on the top. After the heat treatment of the OGE–$SiO_2$–Si substrate *in vacuo*, two comb-shaped gold electrodes were vacuum-deposited on the OGE film. The device structure is depicted schematically in

Fig. 7. The $I-V$ characteristics of the FET were measured using the circuit illustrated in Fig. 7.

In the case of the devices fabricated using the *n*-propyl-substituted OGE as a precursor, no FET amplification was observed. On the other hand, the FET fabricated from the *tert*-butyl-substituted OGE showed signal amplification, where the feature of the FET depended remarkably on the heat treatment temperature of the OGE film.

Figure 8 shows the drain current $I_D$ as a function of drain-source voltage $V_{DS}$ applying different gate bias voltages $V_G$ for the FET fabricated from the *tert*-butyl-substituted OGE film heat-treated at 400 °C. The characteristics of a depletion-mode FET were observed, where the $I_D$ decreased slightly by applying the $V_G$. The current depletion was not enough even at −100 V, which may be due to the top surface conduction. On the other hand, p-channel enhancement-mode FETs were obtained using *tert*-butyl-substituted OGE films heat-treated above 500 and 600 °C.

In Fig. 9, the $I_D$ of the FET fabricated from *tert*-butyl-substituted OGE film heat-treated at 500 °C is amplified by applying the $V_G$. When the negative bias is applied to the gate electrode (silicon substrate), the holes are attracted to the channel between the drain and source. Under the bias condition, the conductivity of the channel between the drain and source is increased, where the channel is called p-channel because the carrier is a hole. The gain of the FET was improved by increasing the heat treatment temperature to 600 °C, as shown in Fig. 10.

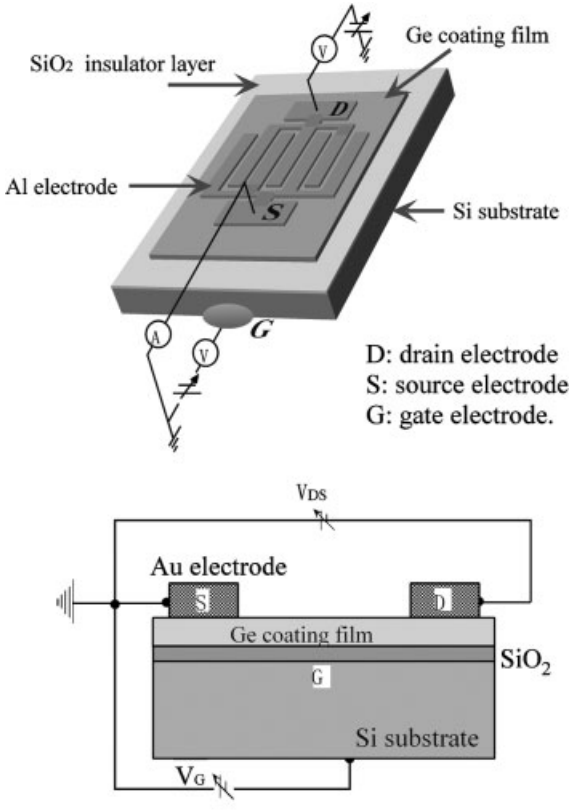


**Figure 7.** Schematic representation of the configuration of the using an OGE film. The channel width and length are 0.1 mm and 31.8 mm, respectively.

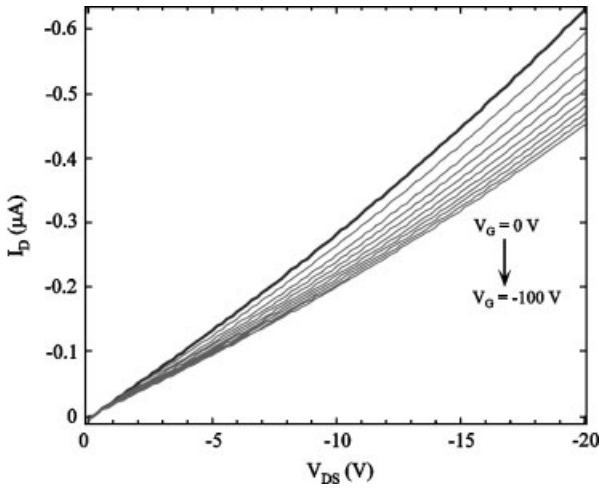


**Figure 8.** $I_D-V_{DS}$ characteristics of the FET fabricated from *tert*-butyl-substituted OGE heat-treated at 400 °C for various $V_G$.

The improvement of the gain can be attributed to the increase in the hole mobility $\mu_h$ with increasing heat treatment temperature of the OGE. When a positive $V_G$ was applied to the FET fabricated from the OGE film heat-treated at 500 or 600 °C, a decrease in the $I_D$ was observed that was assigned to the characteristics of a depletion-mode FET. This result suggests that OGE films heat-treated at 500 and 600 °C are p-type semiconductors and do not show ambipolar conduction.

FETs based on OGEs have some problems. One is the dark current, as shown in Figs 9 and 10, which is a characteristic of germanium owing to the high carrier density compared with silicon.[35] Therefore, germanium semiconducting materials are applied to Si–Ge alloy and heterojunction devices to modify the characteristics of the silicon semiconducting materials. Another problem is that the saturation region of the drain current is not clear in the $I-V$ curve, which may be caused by the heterogeneity of the heat-treated OGE film. If the $I_D$ at $V_{DS} = 20$ V and $V_G = 10$ V is assumed to be the saturation current, then the $m_h$ for the OGEs heat-treated at 500 and 600 °C are estimated to be roughly 0.0154 $cm^2\ V^{-1}\ s^{-1}$ and 0.456 $cm^2\ V^{-1}\ s^{-1}$, respectively using MOS theory for silicon FETs.[27] The mobility is enhanced with increasing heat treatment temperature, i.e. the crystallinity of the germanium.

## CONCLUSIONS

The structural and electrical properties of the OGEs were influenced remarkably by the type of organic substituent. The molecular weight of the *tert*-butyl-substituted OGE was larger than that of the *n*-propyl-substituted OGE. The

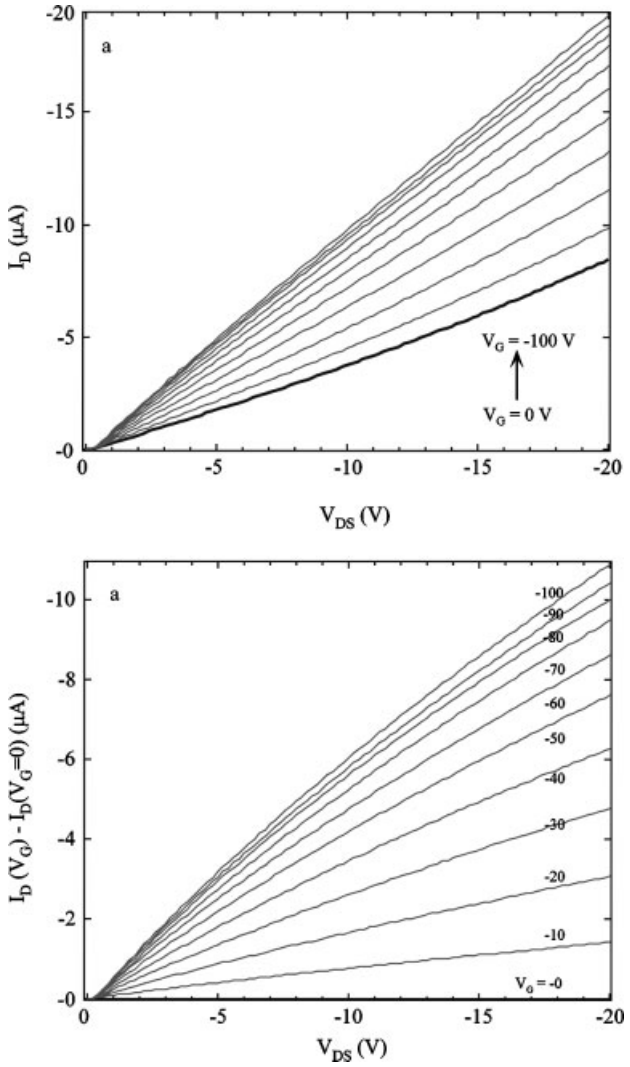


**Figure 9.** $I_D$–$V_{DS}$ characteristics of the FET fabricated from *tert*-butyl-substituted OGE heat-treated at 500 °C for various $V_G$.

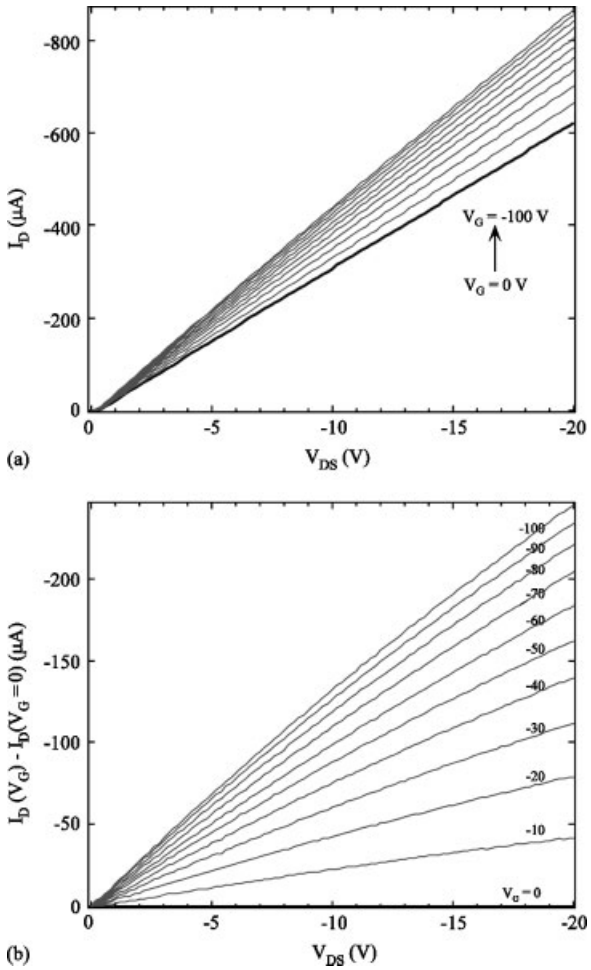


**Figure 10.** $I_D$–$V_{DS}$ characteristics of the FET fabricated from *tert*-butyl-substituted OGE heat-treated at 600 °C for various $V_G$.

ratio of germanium atoms to organic substituents for the former was also higher than that for the latter. These differences can be explained by considering that the bulky *tert*-butyl group effectively surrounds and solubilizes larger germanium clusters in an organic solvent compared with the *n*-propyl group. The optical energy gap of the *tert*-butyl-substituted OGE was lower than that of the *n*-propyl-substituted OGE, which can be attributed to the large extent of the $\sigma$-conjugation along the Ge–Ge chain of the former. Heat treatment enhanced the conductivity of the OGEs, which was induced by the elimination of organic substituents, the reconstruction of the Ge–Ge chain, and the extension of a three-dimensional germanium network among germanium clusters. The FET fabricated by a coating technique using the *tert*-butyl-substituted OGE shows signal amplification properties.

## Acknowledgements

This work was supported by a Grants-in-Aid for Scientific Research (no. 15550179) from the Ministry of Education, Culture, Sports, Science and Technology of Japan.

## REFERENCES

1. Miller RD, Michl J. *Chem. Rev.* 1989; **89**: 1359.
2. Wilson WL, Weidman TW. *J. Phys. Chem.* 1991; **95**: 4568.
3. Bianconi PA, Schilling FC, Weidman TW. *Macromolecules* 1989; **22**: 1697.
4. Furukawa K, Fujino M, Matsumoto N. *Macromolecules* 1990; **23**: 3423.
5. Matsumoto H, Miyamoto H, Kojima N, Nagai Y. *Chem. Soc. Chem. Commun.* 1987; 1316.
6. Watanabe A, Miike H, Tsutsumi Y, Matsuda M. *Macromolecules* 1993; **26**: 2111.
7. Watanabe A, Komatsubara O, Ito O, Matsuda M. *J. Appl. Phys.* 1995; **77**: 2796.
8. Mochida K, Ohkawa T, Kawata H, Watanabe A, Ito O, Matsuda M. *Bull. Chem. Soc. Jpn.* 1996; **69**: 2993.

9. Watanabe A, Fujitsuka M, Ito O, Miwa T. *Jpn. J. Appl. Phys.* 1997; **36**: L1265.
10. Watanabe A, Fujitsuka M, Ito O. *Thin Solid Films* 1999; **354**: 13.
11. Watanabe A, Fujitsuka M, Ito O, Miwa T. *Mol. Cryst. Liq. Cryst.* 1998; **316**: 363.
12. Watanabe A, Unno M, Hojo F, Miwa T. *Mater. Lett.* 2001; **89**: 89.
13. Watanabe A, Unno M, Hojo F, Miwa T. *J. Mater. Sci. Lett.* 2001; **20**: 491.
14. Watanabe A, Unno M, Hojo F, Miwa T. *Chem. Lett.* 2001; 1092.
15. Watanabe A, Unno M, Hojo F, Miwa T. *Chem. Lett.* 2002; 662.
16. Watanabe A, Hojo F, Miwa T, Wakagi M. *Jpn. J. Appl. Phys.* 2002; **41**: L378.
17. Watanabe A. *J. Organometal. Chem.* 2003; **685**: 122.
18. Taylor BR, Kauzlarich SM, Lee HWH, Delgado GR. *Chem. Mater.* 1998; **10**: 22.
19. Taylor BR, Kauzlarich SM, Lee HWH, Delgado GR. *Chem. Mater.* 1999; **11**: 2493.
20. Taylor BR, Fox GA, Hope-Weeks LJ, Maxwell RS, Kauzlarich SM, Lee HWH. *Mater. Sci. Eng. B* 2002; **96**: 90.
21. Garnier F, Hajlaoui R, Yassar A, Srivastave P. *Science* 1994; **265**: 1684.
22. Kuo C, Chiou W. *Synth. Met.* 1997; **88**: 23.
23. Tsumura A, Koezuka H, Ando T. *Appl. Phys. Lett.* 1986; **49**: 1012.
24. Sirringhaus H, Brown PJ, Friend RH, Nielsen MM, Bechgaard K, Langeveld-Voss BMW. *Synth. Met.* 2000; **111–112**: 129.
25. Scheinert S, Paasch G, Pohlmann S, Hoerhold HH, Stockmann R. *Solid-State Electron.* 2000; **44**: 845.
26. Miller RD, Michl J. *Chem. Rev.* 1989; **89**: 1359.
27. Littau KA, Szajowski PJ, Muller AR, Kortan AR, Brus LE. *J. Phys. Chem.* 1993; **97**: 1224.
28. Kurata M, Tsunashima Y, Iwama M. Kamada K. In *Polymer Handbook*, 2nd edn, Brandrup J, Immergut EH (eds). Wiley: New York, 1975; 41.
29. Fok E, Shih M, Meldrum A, Veinot JGC. *Chem. Commun.* 2004; **4**: 386.
30. Graeff CFO, Stutzmann M, Eberhardt K. *Philos. Mag. B* 1994; **69**: 387.
31. Edelman F, Komen Y, Bendayan M, Beserman R. *J. Appl. Phys.* 1992; **72**: 5153.
32. Mulato M, Toet D, Aichmayr G, Santos PV, Chambouleyron I. *J. Appl. Phys.* 1997; **82**: 5159.
33. Vega F, Sema R, Afonso CN, Bermejo D, Tejeda G. *J. Appl. Phys.* 1994; **75**: 287.
34. Watanabe A, Sato TM, Matsuda M. *Jpn. J. Appl. Phys.* 2001; **40**: 6457.
35. Sze SM. *Physics of Semiconductor Devices*. Wiley: New York, 1981.